ACE-FTS Level 0 To 1 Data Processing

Yvan Dutil, Stéphane Lantagne, Simon Dubé, Robert Poulin*
ABB Bomem Inc., SPIR Division, 585 Charest East, Suite 300, Québec, QC, CANADA, G1K 9H4

ABSTRACT

The Atmospheric Chemistry Experiment (ACE) is the mission selected by the Canadian Space Agency for its next science satellite, SCISAT-1. ACE consists of a suite of instruments in which the primary element is an infrared Fourier Transform Spectrometer (FTS) coupled with an auxiliary 2-channel visible (525 nm) and near infrared imager (1020 nm). A secondary instrument, MAESTRO, provides spectrographic data from the near ultraviolet to the near infrared, including the visible spectral range. In combination, the instrument payload covers the spectral range from 0.25 to 13.3 micron. A comprehensive set of simultaneous measurements of trace gases, thin clouds, aerosols and temperature will be made by solar occultation from a satellite in low earth orbit. The ACE mission will measure and analyze the chemical and dynamical processes that control the distribution of ozone in the upper troposphere and stratosphere. A high inclination (74^0), low earth orbit (650 km) allows coverage of tropical, mid-latitude and polar regions.

This paper will describe level 1 algorithms that are needed on ground in order to produce meaningful data meeting all requirements of the ACE FTS instrument. Level 0 data are as downlinked from the spacecraft. Level 1A data are decoded (CCSDS, bit trim) interferograms from individual acquisition channels. Level 1B data are made of spectrally (spatial frequency) calibrated transmittances with annotated quality indicators. Some key ACE FTS L1B algorithms include, non-linearity characterization/correction, robust interferometer fringe count error handling, spectral calibration from Solar reference lines, transmittance computation with phase error correction, and correction of the instrument line shape (ILS) distortion.

Keywords: Infrared, FTS, Space, Algorithms, ACE

1. INTRODUCTION

Atmospheric occultation experiments are conceptually elegant. They involve simply the observation of the Sun outside and inside the atmosphere, plus some observation of the deep space to remove the instrumental emission. However, before extracting scientific information from ACE's data, those need first to be carefully processed to convert them in the appropriate data format and to remove any detrimental instrumental effects. This process is especially extensive in the case of ACE data. Challenging requirements in terms of transmittance accuracy and spectral accuracy imply a careful control of every instrument parameters. Indeed, these requirements cannot be met without the involvement of algorithms.

Even the nature of the experiment itself asks for a very robust data processing. Indeed, having in hand all spectra of the occultation sequence is essential to the extraction of an accurate atmospheric profile. In such circumstance, each interferogram is very precious and need to be manipulated with great care (e.g. the cost of each spectrum is estimated to be more than 100 USD).

In addition, the long nature of the experiment dictates that all processing is done in real time, in order to cope with the continual flow of data. Since, the scientific analysis of the data is in itself quite computationally intensive, we had to optimize the overall calculation process.

* Author to whom correspondence may be addressed, Email: robert.h.poulin@ca.abb.com; Telephone: (418) 877-2944; Web: www.bomem.com. SciSat-1 Web Site: www.science.sp-agency.ca/J3-SCISAT-1.htm.

Earth Observing Systems VII, William L. Barnes, Editor,
Proceedings of SPIE Vol. 4814 (2002) © 2002 SPIE · 0277-786X/02/$15.00

2. DATA PREPARATION

The first step in the data processing is to convert the format of data downlinked by ACE satellite to a more practical format. This involves unpacketizing the CCSDS packet, separate instrument telemetry from FTS, MAESTRO and imager data. Checksums verification insures that no error has been introduced between the instrument and the onboard solid state memory. Also, since FTS data have been encoded onboard using a bit trim mask, bit un-trimming is applied.

3. SPORADIC ERROR HANDLING

Charged particle impacts on the detector produce spikes in the data. Since FTS produces interferogram, those spikes would contaminate the complete spectrum. An obvious method for detecting those spikes is to check for any data points that fill the bit trim mask. However, if this method can detect the larger spikes, it can not detect the lowest energy event that lay below the bit trim mask level. Since the bit trim mask for ACE are conservatively set, a tighter rejection criterion is used for the rejection of anomalous data points.

To refine the spike detection process, we use a sliding window of 512 data points to establish the local statistical properties of the interferogram (mean and standard deviation). We then reject any data point that differs from the average by more than four standard deviations, which should occur statistically less than once per 15 787 data points. The rejected points are then replaced by the bilinear interpolation of their neighbors.

However, this method can only be applied on the tails of interferograms, where there is little oscillation in the signal. Near the central part of the interferogram, the signal oscillates much to rapidly to apply a simple statistical correction scheme. Nevertheless, if a spike occurs in the central part of the interferogram, it is more likely to seriously corrupt the interferogram to the point of rending it unusable. In consequence, those cases will be detected and handle by the data quality control processes.

4. DUAL ADC RECONSTRUCTION

Procurement of analogues to digital converter (ADC) with large dynamic range is difficult for space based application. In consequence, a dual analog-digital converter is used to increase our dynamic range. This allows us to simulate an 18 bits ADC with two 12 bits ADC. One branch of the digitalization circuit use an ADC without amplification the other being amplified by a factor 64 (see figure 1).

Data points for the high gain ADC are used unless saturated. When the high data points are saturated, low gain data are used. Careful characterization of the dual ADC is necessary in order to apply the appropriate gain and offset in the reconstruction process.

This characterization process involves, for each interferogram individually, a comparison between the high gain and low gain data. A robust linear fit allows then to recover the appropriate gain and offset:

$$[m_1, b_1] = \text{LinearFit}\ \left(I_{High}[i], I_{Low}[i]\right). \tag{1}$$

It should be noted that, not only, the saturated data points of the high gain ADC are discarded in the fit, but also the two following data points. This precaution is taken to take account of the recovery time of the ADC after saturation.

The data reconstruction process involves simply the replacement of saturated data and the two following points of the high gain data set by the value of the low gain data multiplied by the gain and added with offset determined in the characterization process.

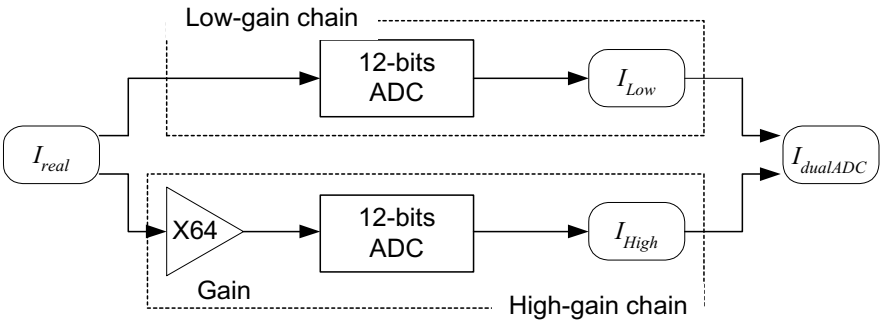

Figure 1: Dual ADC

5. DETECTOR NON-LINEARITY

To reach the required transmittance accuracy, a large flux needs to reach the detectors. In practice, this flux is so high that the detector saturates, its response being no longer linear. This non-linearity affects both MCT and InSb detectors of the FTS. The non-linearity is a local function in the interferogram domain, which translate into a convolution in the spectral domain. In consequence, artifacts appear outside and inside the main spectral band (see figure 2). The artifacts overlapping the spectral band corrupt the spectra and degrade the radiometric accuracy. In ACE, quadratic first and second harmonic and the cubic first harmonic artifacts overlap the spectral band.

We can make use of the presence of those artifacts to characterize the non-linear response of the detector. To do so, the CICM (Convergent Iterative Characterization Method) procedure developed by S. Mueller and F. Cayla from Météo-France, and improved by ABB-Bomem[1]. This method is based on the successive suppression of the band artifacts. First, the non-linearity artifact is set to zero in the spectral domain. In the case of ACE-FTS, only the lower band of the spectral band can be set to zero due to the presence of double modulation in the upper part of the band. This has very little impact on the performance of the method since all artifacts are physically linked together. Once the artifact suppressed is, a modified interferogram is synthesized from the modified spectrum. This interferogram is then compared to the original interferogram. A polynomial fit between the real component of the original interferogram and the synthesized one is applied to determine the non-linearity coefficients. This process is repeated iteratively until convergence. It is important to note that the DC level must be added to the interferogram for the CICM to work. Measuring the DC level is not a simple task on scenes, which significantly vary in brightness within the construction of one interferogram, like the ones observed in solar occultation. For ACE, this is done with a low pass filter that measures the DC level 64 times over the two seconds exposure (ACE-FTS set to high resolution mode).

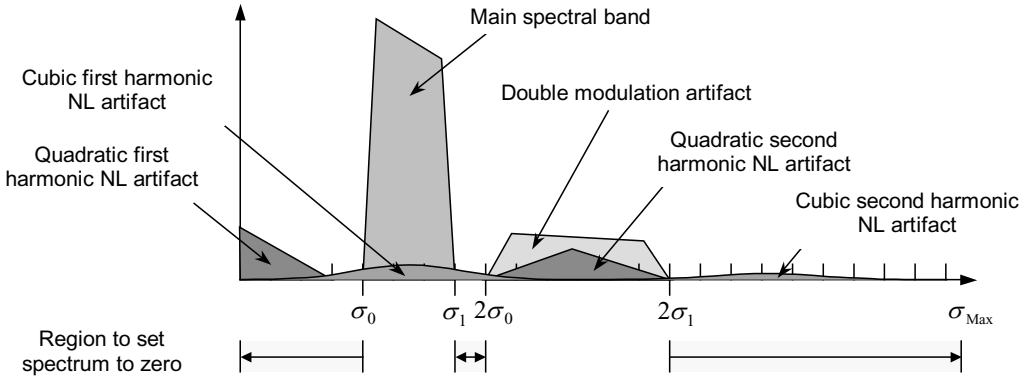

Figure 2: Systematic velocity residual

The non-linearity correction is straightforward since it implies a simple multiplication by a coefficient derived from a polynomial expression. Again, DC level must be added to the interferogram for the correction to work properly. With this method, we have been able to reduce the error associated with the detector non-linearity by more than a factor 30.

6. COMPUTE SPECTRUM

Once the interferogram is reconstructed, the spectrum is calculated. We have chosen the Fastest Fourier Transform in the West (FFTW) to perform the Fourier transform[2]. This algorithm has many advantages. Since it is based on a product of small prime factors, it offers more flexibility than classical "power of two" algorithms. This added flexibility allows us to eliminate the use of zero padding or zero filling, which reduce the correlated noise. For the same reason, this increases the choice of instrumental resolution (see Table 1). In addition, this is one of the fastest algorithms. Prior to the calculation of the spectrum, buffer data points at each end of the interferogram are removed.

Time Interval [s]	MPD [cm]	Spectral Interval [cm^{-1}]	Samples size	
			InSb	MCT
0.1	1.25	0.4	$2^9\,3^2\,7 + 2000$	$2^8\,3^2\,7 + 1000$
0.5	6.25	0.08	$2^9\,3^2\,5\,7 + 2000$	$2^8\,3^2\,5\,7 + 1000$
1.0	12.50	0.04	$2^{10}\,3^2\,5\,7 + 2000$	$2^9\,3^2\,5\,7 + 1000$
2.0	25	0.02	$2^{11}\,3^2\,5\,7 + 2000$	$2^{10}\,3^2\,5\,7 + 1000$

Table 1: Various instrumental configuration

7. FRINGE COUNT ERROR HANDLING

Fringe count error occurs when electronic misses a fringe of the metrology signal when the interferometer turns around. As a consequence of the shift theorem, fringe count error (FCE) produces a linear phase in the spectral domain:

$$I(x-a) \overset{\text{F.T.}}{\leftrightarrow} S(\sigma)\, e^{-2\pi i a \sigma}\,. \tag{2}$$

This phase is added to the natural instrumental phase. If not corrected, FCEs induce large phase errors in the transmittance. Since the resulting erroneous phases can be considered relative between spectra, this property is used to detect and correct FCEs. Relative phase can be easily determined between spectra of the same scene (exo-atmospheric and each deep space spectra). This involves a simple division and a measurement of the linear phase (see figure 3).

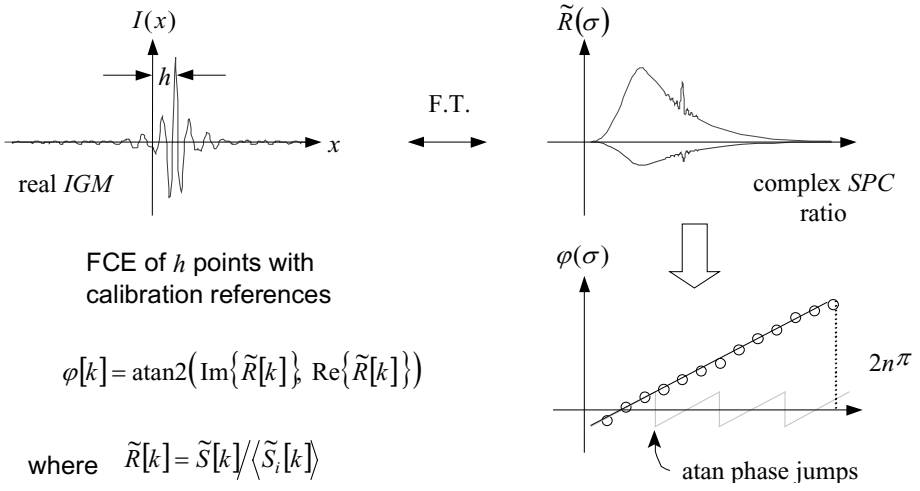

Figure 3: Fringe count error handling

Since there are no two similar atmospheric spectra, a special procedure needs to be applied in order to remove the instrumental phase before searching for the linear phase:

$$\tilde{P}[k] = \frac{\tilde{S}_{\mathrm{S}}}{\langle \tilde{S}_{\mathrm{H}} \rangle - \langle \tilde{S}_{\mathrm{C}} \rangle} = \frac{e^{i\phi_h}(A_{\mathrm{S}} e^{i\phi_{ext}} + A_{in} e^{i\phi_{in}})}{(A_{\mathrm{H}} e^{i\phi_{ext}} + A_{in} e^{i\phi_{in}}) - A_{in} e^{i\phi_{in}}}$$
$$= e^{i\phi_h}\left[\frac{A_{\mathrm{S}}}{A_{\mathrm{H}}} + \frac{A_{in}}{A_{\mathrm{H}}} e^{i(\phi_{in}-\phi_{ext})}\right], \quad (3)$$

$$\tilde{Q}[k] = \frac{\langle \tilde{S}_{\mathrm{C}} \rangle}{\langle \tilde{S}_{\mathrm{H}} \rangle - \langle \tilde{S}_{\mathrm{C}} \rangle} = \frac{A_{in}}{A_{\mathrm{H}}} e^{i(\phi_{in}-\phi_{ext})}, \quad (4)$$

$$\tilde{R}[k] = \frac{\tilde{P}(\sigma)}{\sqrt{|\tilde{P}(\sigma)|^2 - \mathrm{Im}\{\tilde{Q}(\sigma)\}^2} + i\ \mathrm{Im}\{\tilde{Q}(\sigma)\}} = e^{i\phi_h}, \quad (5)$$

where $\tilde{S}_S, \tilde{S}_C$ and $\tilde{S}_H$ are the scene, the cold and the hot reference (here the deep space and the Sun). The factors A_x refer to the respective amplitude of the component. The phases ϕ_{in}, ϕ_{ext} and ϕ_h are respectively the phase of the instrumental emission, the phase of the external sources and the phase shift.

Care must be taken to synchronize the relative phase between the deep space and exo-atmospheric spectra. If those two are not synchronized, residual phase will appear in the scene spectra. In consequence, we synchronize the exo-atmospheric spectra and deep-space by zeroing this function:

$$E_{\mathrm{Im}} = \sum_{k=1}^{N} \left| \mathrm{Im}\left(\frac{\tilde{S}_{\mathrm{S}}[k] - \tilde{S}_{\mathrm{C}}[k]}{\tilde{S}_{\mathrm{H}}[k] - \tilde{S}_{\mathrm{C}}[k]} \right) \right|. \quad (6)$$

Here, the zeroing process implies successive trials with the different fringe count error [0, ±1, ..., ±N] between deep space and solar spectrum to reach $0 + \varepsilon$, where ε is a tolerance value that accounts for noise.

8. SPECTRAL CALIBRATION

Accurate spectral registration inter- and intra-orbit is required in order to fully exploit the high spectral resolution of the ACE instrument. Indeed, the differential nature of an occultation experiment imposes that absorption line fall precisely on the same spectral bin in order to produce an adequate radiometric calibration. This necessity is amplified by the existence of numerous narrow absorption lines in high altitude spectra where the pressure broadening is negligible. Such high precision is normally achieved by the usage of a stable metrology source (e.g. He-Ne laser) or by reference to a gas cell. Unfortunately, those methods were unavailable for the ACE FTS instrument due to power, mass and lifetime constraints. In consequence, we have to produce an absolute spectral calibration on an external reference. For this application the solar spectrum is an obvious reference.

In addition, ACE-FTS uses a laser diode as a metrology source which wavelength can slightly drift with temperature and current variation. Closed loop thermal and electric controls minimize those drifts, but the level of precision required demands further correction. This is provided by dedicated a spectral monitoring algorithm. In consequence, a calibration of the spectral scale is done for each occultation and then, starting from this reference point, a correction is performed for the drift of the laser diode wavelength. Such spectral calibration scheme has also the advantage of taking care of

possible long-term wavelength drifts due to effect of aging and radiation damage on optical components and the laser diode.
To perform the absolute calibration, a simple method is used and is nothing but an application of the "shift theorem". Since the complete discussion of the method is presented elsewhere[3], it is only briefly exposed. On a short section of the spectrum, the Doppler effect and the laser wavelength drift will produce, in first approximation, a shift of the spectral lines. This shift will be translated to a linear phase in the Fourier space, defined as:

$$\phi = \text{Arc tg}\left(\mathsf{F}\,\text{Sun}_{\text{obs}}, \mathsf{F}\,\text{Sun}_{\text{ref}}\right), \tag{7}$$

where Sun_{obs} and Sun_{ref} are the observed solar spectrum and the reference solar spectrum and F is the Fourier transform operator. Note that it is advantageous to use the numerator/denominator form of Arc tg function since this reduces by a factor of two the number of phase jumps.

Once the linear phase is known, the local stretch can be simply calculated as:

$$S \cong \frac{\bar{b}\,\delta\sigma}{2\pi\bar{\sigma}}, \tag{8}$$

where $\bar{b}$ is the average slope, $\delta\sigma$ and $\bar{\sigma}$ are respectively the width and the average wavenumber of the spectral chunk. The final stretching factor is calculated from a weighted average of the stretching factor of every chunk. This weighting factor, following the usual practice, is inversely proportion to estimated variance of *S*, whose value can be derived from the estimated error on the linear phase slope.

It is possible to compensate residual laser wavelength drifts, since the temperature and the current are known to a much better level than the precision of the control system. With an appropriate knowledge of the behaviour of the laser diode, it is possible to do a differential correction from the absolute scale determined on the solar spectrum. Typical laser diodes characterised for ACE-FTS show a wavelength drift of about 11 ppm/mA and 66 ppm/K. In consequence,

$$\lambda_{Diode} = \lambda_{Diode,ref} + \Delta_T \frac{\partial\lambda}{\partial T} + \Delta_I \frac{\partial\lambda}{\partial I} + \Delta_T \Delta_I \frac{\partial}{\partial T}\left(\frac{\partial\lambda}{\partial I}\right). \tag{9}$$

In practice, the precision of the spectral monitoring is limited by the precision of the temperature measurement, which is limited to 10 mK. This value can be improved by averaging the 64 data points taken within the acquisition of one spectrum. This limits our knowledge on relative temperature to 1.25 mK and in consequence our precision on the spectral calibration to 0.083 ppm or 25 m/s.

9. TRANSMITTANCE CALCULATION

The classical definition for the transmittance calculation[4] has been slightly modified to take account of the instrument line shape impact on radiometry:

$$\left(F_{ILS}T'\right)(\sigma) = \frac{\tilde{S}_S(\sigma) - \tilde{S}_C(\sigma)}{\tilde{S}_H(\sigma) - \tilde{S}_C(\sigma)} + \frac{\tilde{S}_H(\sigma) - \tilde{S}_S(\sigma)}{\tilde{S}_H(\sigma) - \tilde{S}_C(\sigma)} \frac{\left(F_{ILS}L_C\right)(\sigma)}{\left(F_{ILS}L_H\right)(\sigma)}, \tag{10}$$

where F_{ILS} is the instrument function describing the impact of the instrument on a monochromatic stimulus (i.e. the instrument line shape, the ILS) on the spectra. In the case of ACE, since the cold reference is the deep space and it has a negligible radiance we have:

$$\left(F_{ILS}T'\right)(\sigma)=\frac{\tilde{S}_S(\sigma)-\tilde{S}_C(\sigma)}{\tilde{S}_H(\sigma)-\tilde{S}_C(\sigma)}. \tag{11}$$

It is assumed here that numerator and denominator spectra are properly resampled on the same spectral grid before the computation of the transmittance. To achieve this, a sinc interpolation algorithm is used.

10. DOUBLE MODULATION CORRECTION

In the case of ACE, the spectral interval covered by each detector is quite large. Since the upper limit of the spectral range of each detector is more than twice the frequency of the lower limit, double modulation contaminates the spectra (see figure 2). The double modulation is produced by a partial reflection of the light on the detector, which is then re-injected in the interferometer to be modulated again, this time twice (back and forth), before returning to the detector. In such circumstance, spectra features are reproduced at twice their original frequency but with a much lower intensity[5,6.]

The difficulty here is to determine the effective reflectivity coefficient of the detector. To simplify this task, two filters (one for each detector) have been selected in order to allow only the lower part of each response band to pass through the interferometer. This allows us to isolate the double modulation component that would be difficult to measure accurately on normal spectra. The reflectivity coefficient can then be measured:

$$\tilde{R}\left(\tfrac{\sigma}{2}\right)\approx\frac{\left(F_{ILS}T'\right)(\sigma)-\left(F_{ILS}T\right)(\sigma)}{\left(F_{ILS}T_{1/2}\right)\left(\tfrac{\sigma}{2}\right)-\left(F_{ILS}T\right)(\sigma)\left[\dfrac{\tilde{S}_H\left(\tfrac{\sigma}{2}\right)-\tilde{S}_C\left(\tfrac{\sigma}{2}\right)}{\tilde{S}_H(\sigma)-\tilde{S}_C(\sigma)}\right]}\approx\frac{\tilde{S}_S(\sigma)-\tilde{S}_C(\sigma)}{\tilde{S}_S\left(\tfrac{\sigma}{2}\right)-\tilde{S}_C\left(\tfrac{\sigma}{2}\right)}. \tag{12}$$

The first order correction can then be applied as:

$$\left(F_{ILS}T\right)(\sigma)\approx\left(F_{ILS}T'\right)(\sigma)-\tilde{R}\left(\tfrac{\sigma}{2}\right)\left(F_{ILS}T'_{1/2}\right)\left(\tfrac{\sigma}{2}\right)+\tilde{R}\left(\tfrac{\sigma}{2}\right)\left(F_{ILS}T'\right)(\sigma)\left[\frac{\tilde{S}_H\left(\tfrac{\sigma}{2}\right)-\tilde{S}_C\left(\tfrac{\sigma}{2}\right)}{\tilde{S}_H(\sigma)-\tilde{S}_C(\sigma)}\right], \tag{13}$$

where

$$\left(F_{ILS}T_{1/2}\right)(\sigma)=\frac{\tilde{S}_S\left(\tfrac{\sigma}{2}\right)-\tilde{S}_C\left(\tfrac{\sigma}{2}\right)}{\tilde{S}_H(\sigma)-\tilde{S}_C(\sigma)}. \tag{14}$$

11. INSTRUMENT LINE SHAPE CORRECTION

Since the field of view of ACE is not infinitesimally small, light rays reaching the detector do not follow the same optical path through the interferometer. This broadens the instrument line shape (ILS) and produces a global displacement of the spectral features toward lower frequencies[7]. In the case of ACE-FTS, the spectral broadening reaches 0.02 cm^{-1} @ 4100 cm^{-1}, i.e. a whole bin at high resolution mode. The mathematical expression for the self-apodization is:

$$S'(\sigma')=\int_0^\infty d\sigma\; F_{SA}(\sigma',\sigma)S(\sigma), \tag{15}$$

where

$$F_{SA}(\sigma',\sigma)=\begin{cases} A & r_c < R_0, \quad \sigma\cos(\alpha_{\min}) \le \sigma' \le \sigma \\ \dfrac{A}{\pi}\arccos\left(\dfrac{\left(\dfrac{\sigma^2}{\sigma'^2}-1\right)f^2+r_c^2-R_0^2}{2r_c f\sqrt{\dfrac{\sigma^2}{\sigma'^2}-1}}\right) & \sigma\cos(\alpha_{\min}) < \sigma' < \sigma\cos(\alpha_{\max}) \\ 0 & \text{elsewhere} \end{cases} . \quad (16)$$

It should be noted that unlike what is sometimes mentioned in the scientific literature this mathematical operation is not a convolution but a Volterra integral of the first kind. In consequence, a simple de-convolution process cannot remove the self-apodization. To resolve this issue, ABB Bomem has developed a correction algorithm based on a linear operator:

$$S[k]=\sum_{k'=0}^{N-1} SA^{-1}[k,k']S'[k'] . \quad (17)$$

It should be noted that this algorithm corresponds to an exact mathematical solution of this inverse problem. In consequence, once the instrument line shape is corrected, the final spectrum possesses exactly the same information content has the uncorrected one. This nice behavior simplifies the conception of the level 2 algorithm. It should be noted that in the case of ACE-FTS, some simplifications are used in order to reduce the size of the matrix to be handle and to speed up the computational process. In any case, the radiometric error introduced by those mathematical artifices is totally negligible.

12. MCT INSB DETECTORS COMBINATION

To increase the signal to noise ratio, transmittance from MCT and InSb detectors can be combined over their common channels. In that case, a weighted average is used:

$$T(\sigma)=\frac{w_{MCT}T_{MCT}(\sigma)+w_{InSb}T_{InSb}(\sigma)}{w_{MCT}+w_{InSb}} . \quad (18)$$

Optimum weight will be determined during the commissioning phase or from ground tests. In any case, the optimum weight is inversely proportional to the level of noise in spectral channels.

13. CONCLUSION

The algorithmic treatment of ACE data from level 0 to 1b provides data as free as possible from any instrumental effects. For the scientific users this means that scientific algorithms can be generalized and do not need any instrument specific data processing. A property very useful when one wants to compare data from different instruments or from many fields of view of the same instrument. Finally, some key algorithms described quickly in this paper have been successfully demonstrated and used for other remote sensing from space projects[8,9], and the level 1b data processing for the ACE mission will have greatly benefit from this heritage.

14. ACKNOWLEDGEMENT

The authors would like to thank Alain Cheli for his useful comments. The Canadian Space Agency supports ACE project.

15. REFERENCES

1. S. Mueller, "Correction of non-linearity and phase error in the IASI interferograms", *Proceeding of the 5th Workshop on Atmospheric Science from Space using Fourier Transform Spectrometry (ASSFTS)*, Tokyo, pp 353-378, 1994
2. M. Frigo and S. G. Johnson, "FFTW: An adaptive software architecture for the FFT," *Proc. ICASSP 1998*, vol. 3, 1381, 1998
3. Y. Dutil, S. Lantagne, R. Poulin, "ACE-FTS Spectral Calibration", *Proceeding Photonics North*, SPIE vol. 4833, Québec, 2002
4. H.E. Revercomb, H. Buijs, H. B. Howell, D. D. Laporte, W. L. Smith and L. A. Sromovsky, "Radiometric calibration of IR Fourier transform spectrometers: solution to a problem with the High-Resolution Interferometric Sounder", *Applied. Optics*, Vol 27., No. 15, 3210-3218, 1988
5. V. Forminsano et al, "Iris Mariner 9 data revisited: 1. An instrument effect", *Planetary and Space Science*, Vol. 48, 569-576, 2000
6. W. E. Ward, Z. Pasturczyk, W. A. Gault, and G. G. Shepherd, "Multiple reflections in a wide-angle Michelson interferometer", *Applied Optics*, Vol. 24, No. 11, 1589–1598, 1985.
7. J. Kauppinen, P. Saarinen, "Line-shape distortion in misaligned cube corner interferometers", *Applied Optics*, Vol 31, no 1. 69-74, 1992
8. R. Poulin, Y. Dutil, S. Lantagne, F. Châteauneuf, "CrIS raw data records (Level 0) to sensor data records (Level 1b) processing", *Proceeding of the Infrared Spaceborne Remote Sensing X*, SPIE vol. 4818, 2002
9. MIPAS, Michelson Interferometer for Passive Atmospheric Sounding, ESA ENVISAT-1 Instrument, `http://envisat.estec.eas.nl/instruments/mipas`.